REPORT DOCUMENTATION PAGE

1. REPORT DATE *(DD-MM-YYYY)*	2. REPORT TYPE	3. DATES COVERED *(From - To)*
22-01-2008	Technical Paper	

4. TITLE AND SUBTITLE

Cavitation-Induced Vibrations in a Two-Bladed Rocket Engine Inducer (Preprint)

5a. CONTRACT NUMBER
FA9300-04-C-0008

5b. GRANT NUMBER

5c. PROGRAM ELEMENT NUMBER

6. AUTHOR(S)
Kevin Burton, Robert Hibbs, Mark Nadolski, & Maria Subbaraman (Aerojet)

5d. PROJECT NUMBER
502603BQ

5e. TASK NUMBER

5f. WORK UNIT NUMBER

7. PERFORMING ORGANIZATION NAME(S) AND ADDRESS(ES)

Aerojet
P.O. Box 13222
Sacramento CA 95813-6000

8. PERFORMING ORGANIZATION REPORT NUMBER

AFRL-RZ-ED-TP-2008-033

9. SPONSORING / MONITORING AGENCY NAME(S) AND ADDRESS(ES)

Air Force Research Laboratory (AFMC)
AFRL/RZS
5 Pollux Drive
Edwards AFB CA 93524-7048

10. SPONSOR/MONITOR'S ACRONYM(S)

11. SPONSOR/MONITOR'S NUMBER(S)
AFRL-RZ-ED-TP-2008-033

12. DISTRIBUTION / AVAILABILITY STATEMENT

Approved for public release; distribution unlimited (PA #08065A).

13. SUPPLEMENTARY NOTES
For publication at the 12th International Symposium on Transport Phenomena and Dynamics of Rotating Machines (ISROMAC-12), Honolulu, HI, 17-22 February 2008.

14. ABSTRACT

Experimental investigation of cavitation induced vibrations in a 2-bladed water model inducer was performed for inlet flowrates ranging from 70% to 120% of the design flowrate and over a range of inlet cavitation numbers representative of a typical rocket engine operation. Dynamic (high frequency) pressure transducers were used to record fluctuating pressures along inducer housing (stationary reference frame) up to 2500 Hz, i.e. about 30 times the shaft speed. Data were obtained in two axial planes: one 0.08 diameters upstream and one 0.37 diameters downstream relative to the inducer blade leading edge tip plane.

Flow visualization data at conditions typical of tip vortex instabilities at high cavitation number and sheet cavitation are presented and correlated to dynamic signature.

Dynamic spectrum of the 2-bladed inducer is compared to data representative of the environment in a 4-bladed rocket engine inducer. The differences in the dynamic characteristics between the 2-bladed and 4-bladed inducers and the potential implications to inducer design decisions for lowering the impact of cavitation induced vibrations in turbomachinery are discussed.

15. SUBJECT TERMS

16. SECURITY CLASSIFICATION OF:			17. LIMITATION OF ABSTRACT	18. NUMBER OF PAGES	19a. NAME OF RESPONSIBLE PERSON
					Sean Kenny
a. REPORT	**b. ABSTRACT**	**c. THIS PAGE**	SAR	11	**19b. TELEPHONE NUMBER** *(include area code)*
Unclassified	Unclassified	Unclassified			N/A

The 12th International Symposium on Transport Phenomena
and Dynamics of Rotating Machinery
Honolulu, Hawaii, February 17-22, 2008

ISROMAC12-2008

CAVITATION–INDUCED VIBRATIONS IN A TWO-BLADED ROCKET ENGINE INDUCER

Kevin Burton, Robert Hibbs, Mark Nadolski
Aerojet, P.O. Box 1322
Sacramento, CA 95813-6000, USA
kevin.burton@aerojet.com
robert.hibbs@aerojet.com
mark.nadolski@aerojet.com

Maria Subbaraman, Aerojet
20750 Ventura Blvd 410
Woodland Hills, CA 91364, USA
maria.subbaraman@aerojet.com

ABSTRACT

Experimental investigation of cavitation induced vibrations in a 2-bladed water model inducer was performed for inlet flowrates ranging from 70% to 120% of the design flowrate and over a range of inlet cavitation numbers representative of a typical rocket engine operation. Dynamic (high frequency) pressure transducers were used to record fluctuating pressures along inducer housing (stationary reference frame) up to 2500 Hz, i.e. about 30 times the shaft speed. Data were obtained in two axial planes: one 0.08 diameters upstream and one 0.37 diameters downstream relative to the inducer blade leading edge tip plane.

Flow visualization data at conditions typical of tip vortex instabilities at high cavitation number and sheet cavitation are presented and correlated to dynamic signature.

Dynamic spectrum of the 2-bladed inducer is compared to data representative of the environment in a 4-bladed rocket engine inducer. The differences in the dynamic characteristics between the 2-bladed and 4-bladed inducers and the potential implications to inducer design decisions for lowering the impact of cavitation induced vibrations in turbomachinery are discussed.

INTRODUCTION

The primary function of an inducer is to facilitate pump operation at high shaft speeds with low inlet pressures. For liquid rocket engines, maximizing pump speed and minimizing inlet pressure lowers overall vehicle weight so more payload weight can be accommodated. This fact makes the inducer a crucial element in net payload lifting cost. As has been recognized early on by Stripling (1962) and Acosta (1962) and confirmed by experience in many different inducer applications involving various working fluids, an inducer's ability to maintain suction at very low inlet pressure (NPSP) improves as its design flow coefficient is reduced. Low flow coefficient inducers have very low blade angles (from tangential) and require a thin leading edge to minimize blade blockage for optimum suction performance. Blade blockage and thus leading edge thickness become key performance factors for such inducers, especially when they operate at high tip speeds. High tip speeds tend to induce high mean-stress levels in the correspondingly thin blading of such low flow coefficient inducers. This high mean-stress condition means understanding the dynamic environment and the unsteady blade loading is critical to rocket engine pump (and engine) life.

Tsujimoto (2001) pointed out that inducer natural frequencies may coincide with the frequencies of vibrations induced by higher order cavitation phenomena that occur at certain operating conditions, including some that fall within the typical operating range of a liquid propellant rocket engine. Such coincidence between blade resonance and cavitation excitation frequencies could conceivably result in structural failure. Further, multiple cases of structural damage to both pump and surrounding hardware have been cited in recent years wherein cavitation instabilities were believed to play a role. It is therefore desirable to understand and predict the nature and behavior of these potentially destructive cavitation forces.

.

NOMENCLATURE

A   Amplitude of pressure oscillations
Amax   Maximum amplitude of pressure oscillations
D   Inducer tip diameter
h   Circumferential blade spacing at tip ($\pi D/Z$)
Hanover Plot of phase vs transducer clocking in a plane
HORC   Higher Order Rotating Cavitation
HOSC   Higher Order Surge Mode Cavitation

LE   Inducer leading edge
LH2   Liquid hydrogen
LOX   Liquid oxygen
N   Shaft speed, rpm
NPSH   Net positive Suction Head (ft)
NPSP   Net positive suction pressure = Pinlet –Pvapor,
PCB   A brand of high frequency transducer
Pv   vapor pressure
Qdes   Inducer volumetric flowrate at design point,
RC   Conventional rotating cavitation (at about 1.05- 1.6N)
x   Dimensionless axial distance from inducer LE at tip normalized with inducer tip diameter D

1

Z	Number of inducer blades
α	Incidence angle relative to blade pressure side in radians = (blade angle – flow angle) (Angles measured from tangential direction)
ϕ	Flow Coefficient at inducer inlet (with hub blockage)
ϕ_des	Inducer Design Flow Coefficient
σ	Cavitation number based on total pressure = (Ptotal-Pvapor)/0.5*density*Utip^2

TEST ARTICLE AND TEST SET-UP

The data presented herein is for a 111.8mm (4.4in) tip diameter aluminum model of a 2-bladed, unshrouded inducer tested with a straight, constant diameter inlet. The test article is a scaled up model an inducer designed for a relatively small liquid hydrogen pump. The water model test program for this inducer had many objectives, including hydrodynamic performance, axial and radial load assessment, thermodynamic effects (hot water testing) and validation of performance prediction tools. Dynamic environment characterization was not the primary objective of the test, and only limited dynamic data was obtained.

Figures 1 and 2 show the overall test setup and a close-up view of the inducer test section, respectively. The insert in Figure 1 is the front view of the 2-bladed inducer.
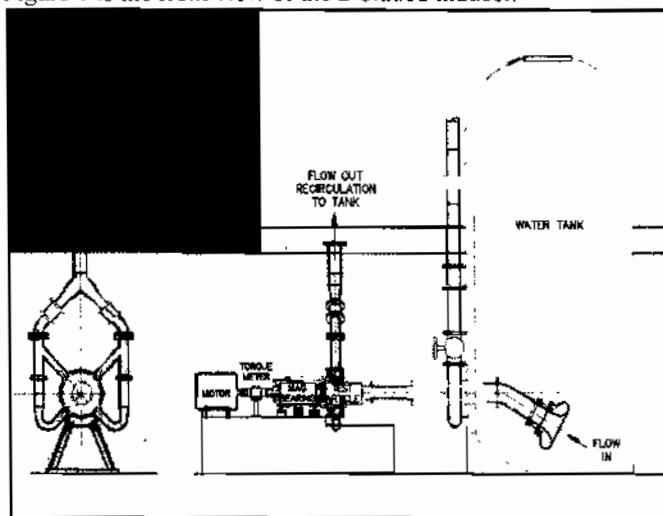

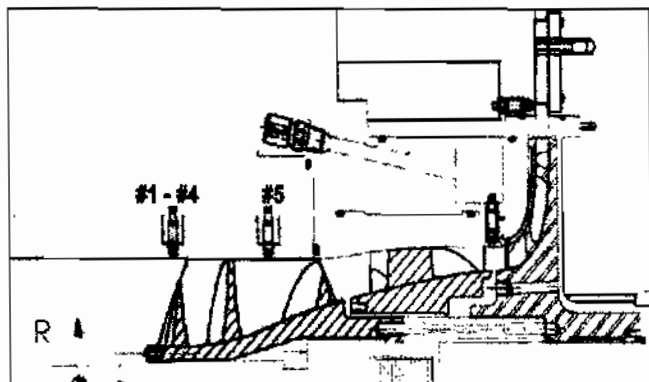Figure 1: Test set-up overview

Figure 2: Inducer test-section showing 4-PCB array near inducer leading edge

The inducer was driven by an electric motor, at a constant shaft speed of N=5000rpm, resulting in a constant inducer tip speed of about 29.3 m/s (96 fps). The inducer shaft was supported on magnetic bearings which allowed for measurement of steady and unsteady shaft reaction loads in both the radial and axial directions. The inducer shaft was connected to the electric motor using a coupling located between the magnetic bearing unit and the electric motor. Test water was supplied from a large tank equipped with pressurization and vacuum systems. Water temperature was typically about 22 deg C (74 deg F). Tank water was de-aerated before each cavitation test and oxygen content was maintained at or below 4ppm.

Figure 3: Flow visualization set-up at Concepts NREC

As shown in Figure 3, an acrylic window giving partial view of the inducer was used for flow visualization. Two of the four dynamic pressure transducers at the inlet plane were placed on the acrylic window within view of the test article, and the rest were on the aluminum tunnel. Video recordings, including some with sound, were performed at all operating flow coefficients and over a wide range of cavitation numbers. Continuous video recording was performed starting at high inlet pressures corresponding to the "non-cavitating" inducer head rise, down to a full cavitation head breakdown.

INSTRUMENTATION & TEST PROCEDURE

High frequency dynamic pressure measurements were obtained for discrete flowrates of 70%, 85%, 100%, 110% and 120% of design, using PCB high-frequency pressure transducers located at two axial locations: -0.08D, and -0.37D relative to the inducer leading edge at its full tip diameter. Four PCB's (#1 - #4 in Figure 2) immediately upstream of the inducer blade leading edge (-0.08D location) were arranged in an asymmetric array to facilitate phase analysis and to preclude spatial aliasing, as shown in Table1.

All PCB's were rated for 1000 psi, with -/- 1 psi resolution. Transducers with a 1000 psi static pressure rating were selected even though the maximum static discharge pressure was significantly lower. This was done to maximize survivability in deference to accuracy considering the localized

2

dynamic pressure extremes anticipated near the inducer leading edge. All pressure transducers survived the testing without failure.

Table 1: Axial location and clocking of pressure transducers

PRESSURE TRANSDUCER	AXIAL LOCATION – RELATIVE TO INLET	CIRCUMFERENTIAL LOCATION – RELATIVE TO PROBE 1
1	0.08D upstream	0 degrees
2	0.08D upstream	100 degrees
3	0.08D upstream	220 degrees
4	0.08D upstream	333 degrees
5	0.37D downstream	100 degrees

In addition to using dynamic pressure data, the readings from the magnetic bearing currents were used to help establish phase relationships.

The force in the actively controlled magnetic bearings used in this study is created by the current in windings around electro magnets placed along the periphery of the rotor. Forces on the rotor are inherently unstable because as the gap between the electromagnets and the rotor decreases, the force increases, requiring a control system with rotor position as input and current through the windings of electro magnets on opposing quadrants as file output. Controllers on each axis control the current, i.e. control the force, to keep the rotor in the required position. The two radial magnetic bearings and axial magnetic bearings are used to position the rotor and measure displacements and forces. Reaction forces along each axis are measured by correlating the current and position from the controller to a calibrated force model.

At each flowrate the inlet pressure started out high and was gradually reduced until inducer head dropped by at least 30%. This was performed per planned experimental procedure. Flowrate was manually adjusted during cavitation testing to maintain a constant flowrate as inlet pressure was varied. During each flowrate test-run steady-state data (e.g. static pressure, temperature, etc.) were recorded at multiple discrete times, while high-frequency unsteady pressure data was recorded continuously.

RESULTS AND DISCUSSION

The dynamic data of the 2-bladed inducer were studied at time slices either exhibiting large magnitudes in the spectral plots or, to a lesser extent, at flow conditions exhibiting cavitation instabilities historically, in 4-bladed and 3-bladed inducers. General observations are given first, followed by a discussion of higher order cavitation instabilities.

General observations

Numerous discrete frequencies were observed, varying in amplitude as the cavitation number changed over the course of the run. Figure 4a shows data at 100% Q/N design, at the location 0.37D downstream of the inducer leading edge tip, and Figure 4b shows data at the same operating point at both axial positions, -0.08D (labeled "Upstream) and +0.37D (labeled ("Downstream") relative to the LE tip, together with line plots of the cavitation number σ and the $\sigma/2\alpha$ parameter. Frequency is

plotted along the abscissa, with time along the ordinate. Amplitude is represented by color intensity, with green and blue as the lowest, and yellow and white as the maximum. The bottom of the plot corresponds to the beginning of the test, where inlet pressure is a maximum. Classic cavitation associated with head breakdown occurs at the top edge of the plot, near the end of the test run. Note the increase in spectral content at this axial position as inlet pressure is reduced.
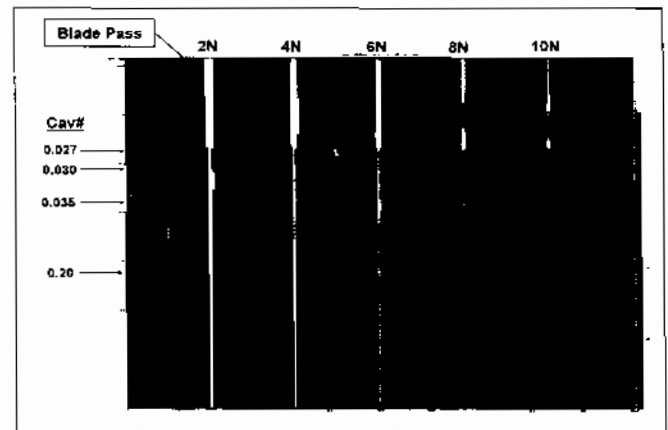

Figure 4a: Fluctuating wall pressure spectrum at 100% design flowrate at 0.37D downstream of inducer leading edge tip

The region of greatest spectral activity occurs for σ ranging from about 0.20 to ~0.08, well above where head breakdown was observed. This contradicts the prevailing notion that the most severe dynamics occur during "deep cavitation" (associated with head breakdown). Although the blade passing frequency discretes reach maximum amplitudes closer to the breakdown point later on in the test, such strong discretes alone are not particularly deleterious because they occupy a narrow portion of the overall spectrum, remain at a fixed ratio of shaft speed, and are classically accounted for in current design methodology. Figure 4a also illustrates the tendency for exclusivity observed in other inducer data (Bordelon (1995), Tsujimoto (1997) and others). That is to say: only one family of frequencies (associated with a specific waveform) tends to exist for any given operating condition, and only after that family of frequencies dies out, does another family appear.
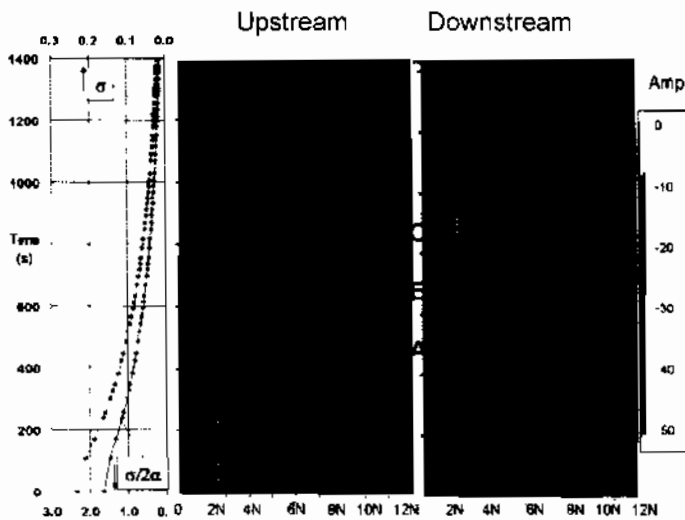
3

Figure 4 b: Fluctuating wall pressure spectrum at 100% design flowrate at -0.08D and 0.37D relative to inducer leading edge tip and corresponding σ and σ/2α
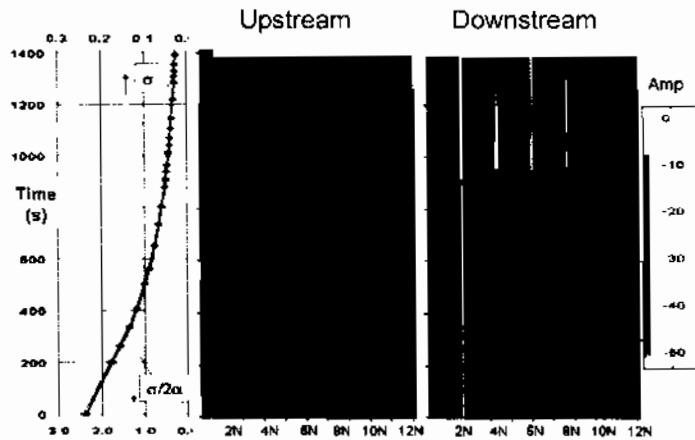

Figure 4c: Fluctuating wall pressure spectrum at 120% design flowrate at -0.08D and 0.37D relative to inducer leading edge tip and corresponding σ and σ/2α
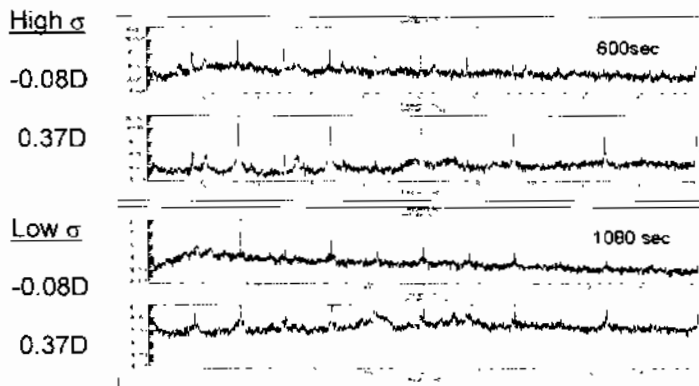

Figure 5: Relative dynamic pressure amplitudes in -0.08D & 0.37D planes at 100% φ_des at two different levels of σ
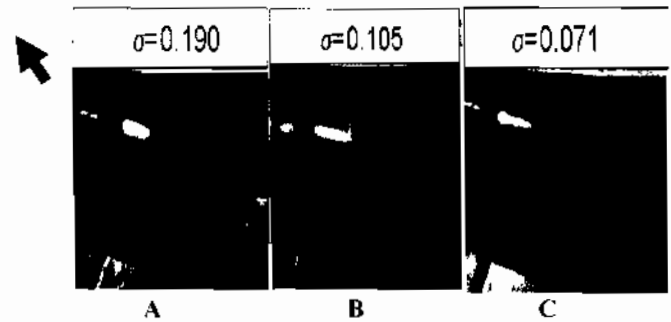

Figure 6: 2-bladed inducer flow visualization at 100% of design flow coefficient and different cavitation numbers

Figure 4b shows a significant difference in dynamic environment between the two axial locations at virtually all σ. The right hand side of Figure 4b shows the same data as Figure 4a, but in a different color scale. At 0.08D plane (left hand side) the overall level of dynamic activity is higher at σ>0.1, whereas the trend in the ~0.37D plane is opposite, i.e. dynamic pressure amplitudes show a tendency to increase with decrease in σ. This is probably due to the fact that at high σ tip vortex cavitation is dominant, and tip vortex cavities form in the tip region at the leading edge and just upstream of the leading edge of the inducer. At lower cavitation numbers tip vortex cavitation extends deeper into the inducer, and usually sheet cavitation is also present, affecting the tip vortex.

Figure 4c shows the dynamic spectrum at 120% φ_des (highest tested). The colors in the spectral plots are not based on the same scale. Figure 5 shows line plots of dynamic pressure amplitude vs. frequency for the upstream and downstream data at 2 time slices. At 600 sec (high σ), the upstream and downstream amplitudes are similar and the upstream amplitudes are is higher over some frequency range, but at 1080 sec (low σ), the downstream amplitudes are higher over most of the spectrum.

At 120% φ des the intensities of 1N, non-blade wake shaft harmonics and asynchronous discretes increase at σ−~0.084 to~ 0.012. Synchronous energy is normally associated with mechanical unbalance, but in this case it is clearly being driven by hydrodynamics (since inducer mass distribution is not changing throughout the test run). Thus hydrodynamics must be

considered before attributing elevated synchronous energy to purely mechanical causes in a health monitoring situation.

Figure 6 shows flow visualization photos at 100% design flow. Tip vortex cavitation changes with σ appear consistent with dynamic data. Flow visualization did not show clear evidence of sheet cavitation at any value of σ. This is unusual, however the sheet cavity may not have been visible due to the viewing angle.

The letters A, B, C in Figure 4b correspond to the the visualized conditions marked by the same letters in Figure 6. Note that zone A, with highest level of activity in the -08D plane has a very small tip vortex cavity. The transition from zone B to zone C is characterized by a sudden broad-band drop in activity level in the upstream plane, and an increase in dynamic activity in the downstream plane.

Flow visualization photos in Figure 6 show that this change in the dynamic characteristic corresponds to an abrupt expansion in vapor volume and a jump in the extent of visible cavitation. In zone A the cavitation appeared to be a tip vortex type, extending only a short distance upstream of the leading edge tip. However, in zone B, i.e. at $\sigma<0.1$ the visible cavitation extends over the full axial length of the inducer. For $\sigma>0.1$ in Figure 4b the data at -0.08D location shows elevated activity at frequencies exceeding 10 times the shaft rotational frequency, whereas at lower σ the activity is limited to lower frequencies for that axial position.
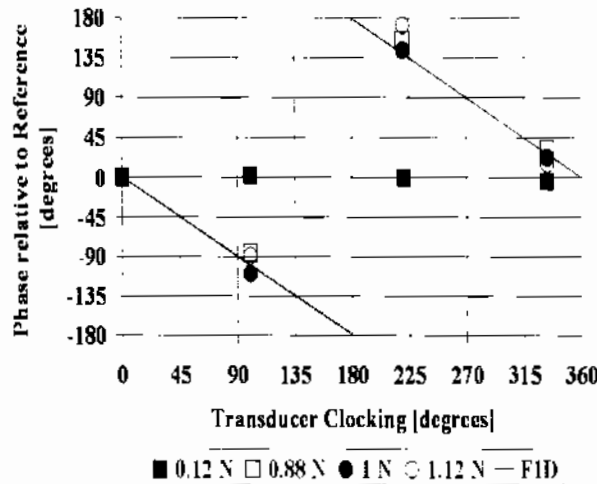

Figure 7: Hanover plot of the of 0.08D upstream ring of pressure transducers at the design flow coefficient

Figure 4a shows a high level of "side band" activity at about 900 sec, suspected to be rotating cavitation or cavitation surge related. Phase analysis over this time frame was performed. Figure 7 is a Hanover plot at the 100% ϕ_des, at $\sigma=0.082$, where sideband activity is greatest. For each of the four transducers in the array at -0.08D, a linear cross-coherence analysis was performed over the timeframe associated with a cavitation number of 0.082 using the zero-degree transducer as a common reference. The resulting phase angles relative to the reference transducer is plotted on the ordinate, with transducer position (angle) plotted on the abscissa. Several different

discrete frequencies are plotted, with the forward-1D line (corresponding to a forward-precessing single-cell disturbance) shown for reference. Synchronous energy associated with mechanical unbalance should lie right on the forward-1D line as it does here. The asynchronous sideband frequencies roughly tracking speed at approximately 0.88N and 1.12N also lie right along the forward-1D line, indicating a single-cell hydrodynamic disturbance rotating in the same direction as shaft rotation, characteristic of rotating cavitation.

Rotating cavitation has been documented on 3-blade and 4-blade inducers and a similar "rotating stall" phenomenon at 0.31N and 1.69N is cited on an a 2-bladed inducer design called "FAST2" (Cervone (2002). On 4-bladed inducers rotating cavitation tends to constitute the majority of the energy in the spectrum (from DC to beyond 2x blade-pass). However, in the case of the subject design as well as the FAST2 case the rotating cavitation phenomenon does not appear to dominate the spectrum.

More cases are necessary to conclusively establish an accurate correlation. Developing such correlations is desirable because these cavitation instabilities impart significant loads to the inducer blading as well as to the rotor, bearings, and surrounding structure. Unlike commercial hardware where design margins are relatively conservative, rocket engines are designed with much lower structural margins, mandating a more detailed understanding of the loading environment to ensure safe, reliable operation over the life expectancy of the machinery.
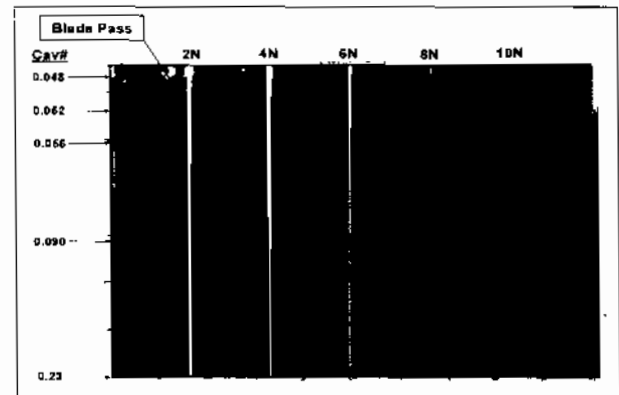

Figure 8: Fluctuating wall pressure spectrum at 70% design flowrate 0.37D relative to inducer leading edge tip

A dynamic pressure spectrum at 70% design flowrate (the lowest tested) is shown in Figure 8. The spectrum associated with this low, off-design, flow coefficient exhibits rising random energy with decreasing cavitation number.

5

As pointed out by Tsujimoto (2001) and confirmed by many others, tip vortex cavitation instabilities are associated with higher order cavitation phenomena, discussed separately below.

Higher Order Cavitation Instabilities.

Higher order cavitation instabilities in rocket engine inducers are of special interest, because:
-       They occur at cavitation number and flowrate ranges (and thus $\sigma/2\alpha$ range) typical of rocket engine operation at full power level in flight
-       They are characterized by a surge mode (in addition to rotating modes), with a capacity to travel far upstream and far downstream of the inducer, with the potential to impact distant elements of the engine system
-       Higher order cavitation instabilities are characterized by high frequencies (several times the shaft speed) and by higher harmonics and many modulations with blade passing frequency and other discretes spanning wide frequency range, increasing the risk of unanticipated high cycle fatigue failures

In the last few years progress has been made in characterizing and understanding higher order cavitation instabilities, including both simple helical geometries and some real engine hardware (Tsujimoto (2001), Fujii (2002), Subbaraman (2003)).

With the increased understanding of their potential deleterious effects on hardware, many attempts have been made to eliminate different types of cavitation induced vibrations. A number of different passive and active flow-altering devices were proposed and tested, usually involving the inlet section and/or inducer housing geometry: (Horiguchi (2000), Rebattet (2001), Yoshida (2001), Shimura (2003), Imamura (2003), Ono (2004), Subbaraman (2006), Kim (2006), Shimiya (2006).

It is of interest, therefore, to establish if a 2-bladed inducer design offers advantages relative to 4-bladed designs in regard to higher order cavitation instabilities. The dynamic data was therefore scrutinized at $\sigma/2\alpha$ conditions where HOSC-HORC instabilities have been observed in 4-bladed inducers.

Figure 9 (Subbaraman (2006)) shows progression of cavitation phenomena and associated vibrations with σ typical to 4-bladed inducers. The data shown is for a moderate flow and head coefficient 4-bladed inducer operating slightly above its design flow coefficient. In contrast to the overall objectives of the 2-bladed inducer test program discussed herein, where dynamic characterization was relatively low priority, the 4-bladed inducer was tested specifically for the purpose of characterizing and understanding its dynamic environment. Therefore, unlike the typical cavitation testing, with test runs at flowrate increments of 10%, the 4-bladed inducer was tested at much finer increments of about 2% of the design flow (near the region of interest). In addition, dynamic pressure transducers were placed in several planes very close to the inducer leading edge tip. This allows capturing HOSC-HORC amplitudes at their peak. (Although HOSC propagates far upstream and downstream, its amplitudes vary greatly with axial position.) Several PCBs were used in each plane to facilitate spatial characterization of the wave form.
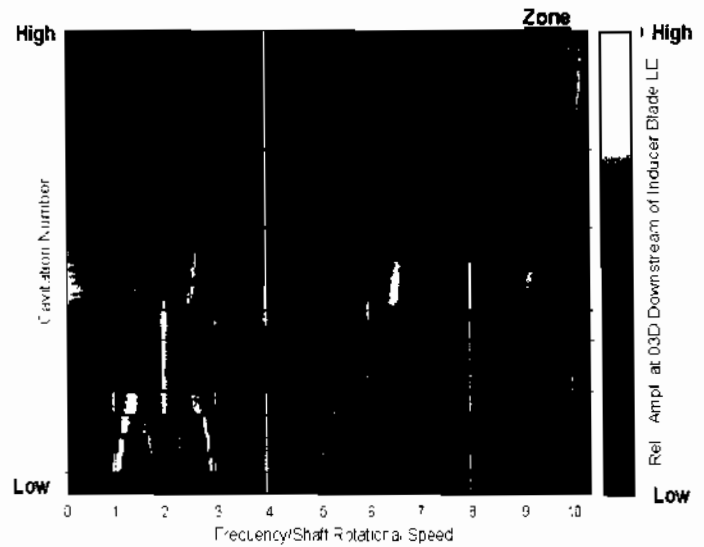

Figure 9: Progression of cavitation induced vibrations in a 4-bladed inducer at $\phi=1.02 \phi\_des$ (highest cav# at top of figure. Operating ϕ and PCB plane are at the peak of higher order surge and rotating cavitation (HOSC-HORC)
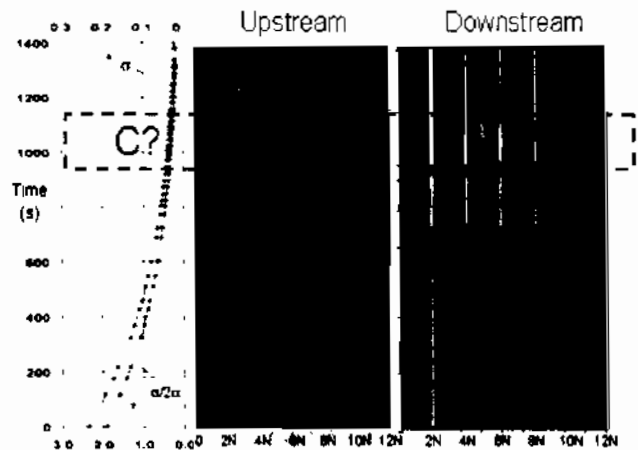

Figure 10: Progression of cavitation induced vibrations in the 2-bladed inducer at $\phi=1.10 \phi\_des$ (highest cav# at bottom of figure) Operating ϕ and PCB planes are not at the peak of higher order surge and rotating cavitation (HOSC-HORC)

Letters A through H in Figure 9 denote operating zones characterized by different and distinct cavitation phenomena. The 2-bladed inducer data was examined specifically looking for HOSC-HORC at all operating flow coefficients.

Potential HOSC-HORC instabilities were noted in the data at 110% and 120% of the design flow coefficient at similar discretes. The spectrum at 110% design flowrate is given in Figure 10, and the data at 120% design flow is shown in Figure 4c. A dashed line rectangle in Figure 10 marks the zone that has some similarity to zone C (i.e. the HOSC-HORC zone) for the 4-bladed inducer shown in Figure 9.

Strong ~6.5N discretes are seen in the downstream plane at 0.37D, where there was only one PCB. The signal

6

strength in that frequency range in the upstream plane, where there were 4 PCBs, is very weak, and it was not possible to discern any information regarding the wave form from that data.

One unique aspect of the subject 2-bladed inducer test set-up is the use of magnetic bearings. They were used for radial and axial load assessment of the overall pump. The magnetic bearings were operating in "active control" mode at all times to maintain rotor concentricity and prevent axial movement. It is conceivable that the active control mode interfered with the "normal" development of cavitation induced vibrations in this inducer. On the other hand, magnetic bearing control currents measurements provided another type of data, which was utilized as discussed below.
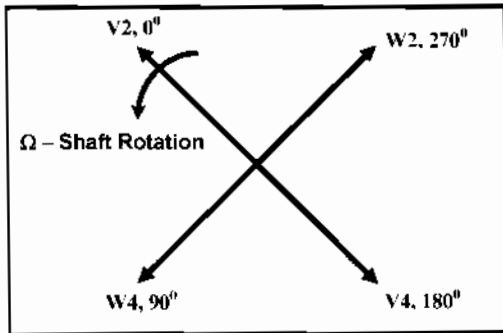

Figure 11: Magnetic bearing control current orientation

Magnetic bearing control currents were used to establish if the instabilities where rotational in nature and their direction of rotation relative to the inducer rotation. The magnetic bearing control currents were recorded along with the dynamic pressures. The control currents of the bearing closest to the inducer (V2, W2, V4 & W4) were used to assess the phase relationship. The orientation of these currents is shown in Figure 11. Because the magnetic bearing would react any cavitation instability loads represnted in the pressures, the phase relationship between these currents was used to assess if the instability was rotating with the inducer and, if so, its rate.
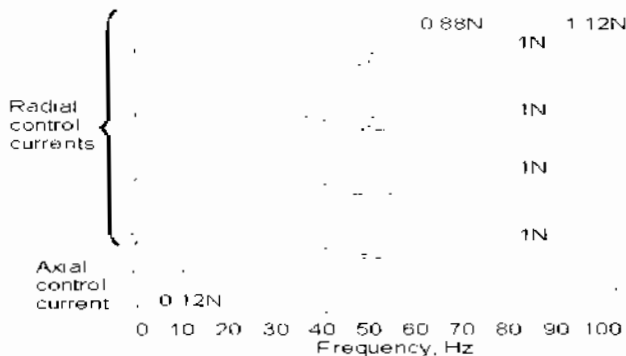

Figure 12: Auto spectrum of 4 radial control and one axial control currents at 100% design flowrate during cavitation surge

Figure 12 is a plot of radial and axial control current measurements vs. frequency generated, as a check, for 100% design flowrate at the time slice where dynamic pressure data

established a presence of a strong surge mode at 0.12N. As has been shown in Figure 7 (Hanover chart), in addition to 0.12N surge, 3 forward rotating modes at 0.88N, 1N and 1.12N were present at the same time. The radial control currents data in Figure 12 is consistent with the phase relationships in Figure 7, showing the 3 rotating modes. The axial control current data has a strong signal at 0.12N surge, as expected, but it also shows a peak at 1.12N, where only rotating modes were detected in the pressure data. Therefore it appears that the axial control current data cannot be depended upon for surge detection.
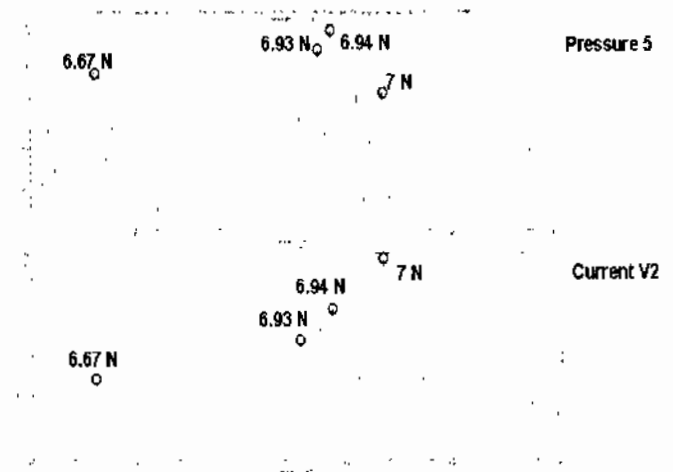

Figure 13: Auto spectrum of 0.37D pressure and V2 current at flow coefficient of 110% of design and cavitation number of 0.022

Figure 13 shows the auto spectrum of dynamic pressure No. 5 (at 0.37D) and magnetic bearing current V2. Note that the pressure spectrum corresponds to the magnetic bearing control current. The coherence for the labeled points is greater than 0.94

A Hanover plot showing the phase relationship is shown in Figure 14. Note that the instability seen at 6.93N and 6.94N appear to be rotating forward at shaft speed and the instabilities at 6.67N and 7N appear to be rotating backward at shaft speed. The rotating components of the HOSC-HORC instability often have both forward and backwards modes, but usually they would have a surge mode in the middle. In this case HOSC would be expected to exist at f=~6.8N, where dynamic pressure amplitude shows only a small local peak. The surge mode, if present, could not be detected using magnetic bearing currents measurements in this radial plane.
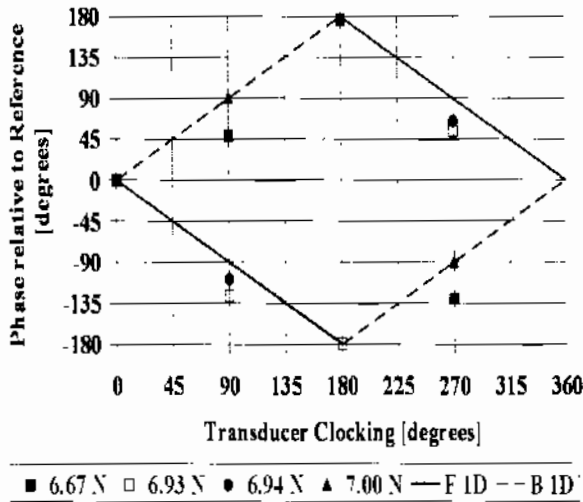
Figure 14: Hanover plot of magnetic bearing currents for flow coefficient of 110% of design and cavitation number of 0.022

Figure 15: Hanover plot of magnetic bearing currents for flow coefficient of 120% of design and cavitation number of ~0.029

Coherence in relation to the V2 current was assessed for the other control currents and shown to be greater than 0.99 for the 6.93N and 6.94N discretes and greater than 0.97 for the 7N discrete. For the 6.67N discrete the off axis currents, W2 and W4, only had coherences of 0.83 and 0.87 respectively while the V4 current is 0.99. The coherence relative to the V4 current should be high because the V2 current and the V4 current have the same controller.

The dynamic spectrum at 120% ϕ des shown in Figure 4c indicates a discrete at around 6.5N for σ= 0.027 to 0.029, and a weaker discrete at ~4.5N.. These two discretes are plotted in a Hanover chart in Figure 15. Both of them were found to be rotating synchronously backward.

The FAST2 data (Cervone (2002)) indicated a surge mode at ~4.4N attributed to higher order cavitation, and a concurrent ~6.6N mode. Present authors estimated the σ/2α of that data was about 0.2, which is relatively high. To put it in perspective, in the case of the reference 4-bladed inducer, σ/2α=0.2 would correspond to the 10-10.5N vibration, and is about 4 times higher than σ/2α corresponding to HOSC-HORC for that inducer (Figure 9). It is therefore concluded that FAST2 inducer did not exhibit the classic HOSC-HORC.

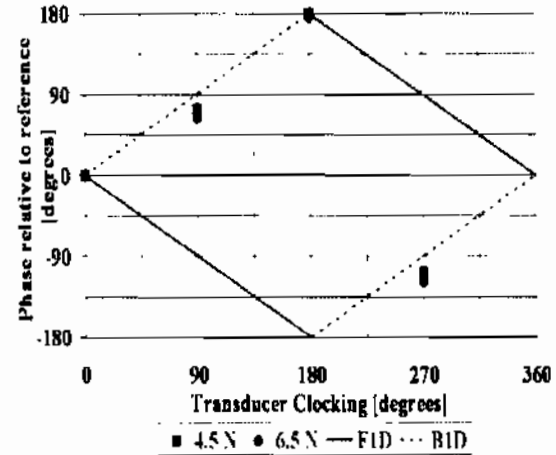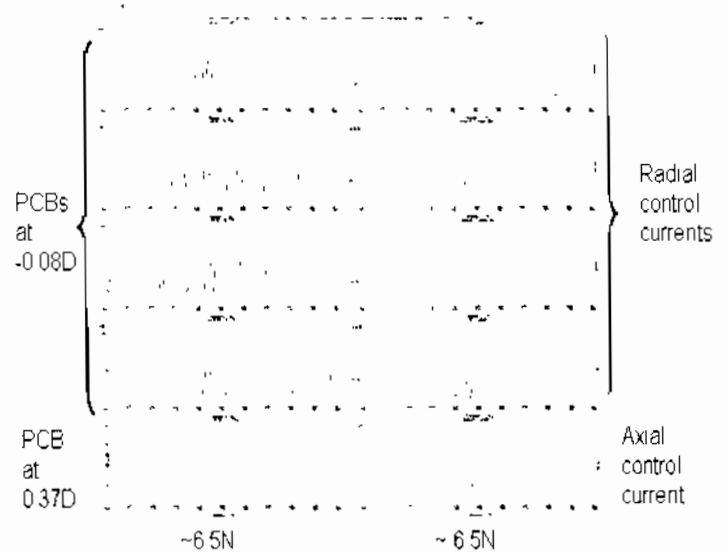Figure 16: Dynamic pressure data and magnetic bearing control current measurements at 120% design flowrate at time slice of strong ~6.5 discretes (σ/2α=~0.5)

Figure 16 shows a comparison between the dynamic pressure data at both upstream and downstream positions and the radial and axial magnetic bearing control current measurements at 120% design flowrate at the time slice of strong ~6.5 discretes, where σ/2α is within the HOSC-HORC range in 4-bladed inducers. An interesting data point is the axial control current showing a strong signal at that same shaft speed ratio. However, as concluded based on comparison of Figure 7 and Figure 12 phase data, this data is not reliable for surge detection. It does however suggest, that, perhaps, some inducer axial motion tendency is being suppressed.

In summary, higher order rotating cavitation with both forward and backwards rotating modes was observed at $\sigma/2\alpha$ values typical of HOSC-HORC instabilities in 4-bladed inducers, but at somewhat lower σ and at ϕ/ϕ_des somewhat higher than those of higher order surge and higher order rotating cavitation typically seen in 4-bladed inducers. However, the frequency to shaft speed ratios of these instabilities, at about 6.5 to 7.0, were very close to those seen in 4-bladed inducers. Furthermore, the difference between the forward and backwards rotating modes of about 0.3N is also similar to that observed in some 4-bladed inducers

.The higher order surge cavitation mode (HOSC), which usually is prominent in 4-bladed inducers and has f/N in-between the forward and backwards rotating modes, was not detected in this test data.

Higher order surge cavitation is of great interest in characterizing the dynamic environment of rocket engine inducers, because this mode has the capacity to modulate into many frequencies and affect remote system components both upstream and downstream of the inducer. It would, therefore, be important to establish if this 2-bladed inducer does not exhibit HOSC by virtue of its design preventing this type of tip vortex instability, or whether available data is inadequate to detect it.

CONCLUSIONS

Preliminary assessment of cavitation induced vibrations in a 2-bladed LH2 inducer water model was performed for a range of flowrates from 70% to 120% of design. Cavitation surge, asymmetric cavitation and various modes of rotating cavitation were identified at most flowrates.

Good correlation was established between magnetic bearing control currents data and dynamic pressure phase data for rotating wave forms.

Higher order rotating cavitation modes (backward and forward) were detected at frequency to shaft rotational speed ratios similar to those seen in 4-bladed inducers, but at higher ϕ/ϕ _des and at somewhat lower cavitation number and $\sigma/2\alpha$.

Higher order surge cavitation that typically accompanies the higher order rotating modes in 4-bladed inducers was not detected.

The test data for this 2-bladed inducer alone is insufficient to conclude whether 2-bladed inducers inherently do not exhibit HOSC, or whether it was suppressed or missed. This points out to a need for establishing standards and guidelines for dynamic testing of inducers to ensure valid and complete characterization of all forms cavitation induced vibrations.

Higher order surge cavitation is probably the most potentially damaging form of cavitation instability in rocket engine inducers. If it can be established that 2-bladed inducers do not exhibit HOSC, the 2-bladed designs would be safer and thus preferable for rocket engine application. This test data alone is not sufficient to prove this. However, suitable test data may already exist, or could be obtained relatively easily. Obtaining such data and scrutinizing it to determine if 2-bladed inducers are potentially safer than 4-bladed would be worthwhile.

REFERENCES

Bordelon, Jr., W.J., Gaddis, S.W., and Nesman, T.E., "Cavitation Environment of the Alternate High Pressure Oxygen Turbopump Inducer," ASME FED-Vol. 210,39-46, 1995

Cervone, A., Torre, L., Bramanti, C., Rapposelli, E., Agostino, L., Experimental Characterization of Cavitation Instabilities in the Avio "FAST2" Inducer, 41st AIAA/ASME/SAE/ASEE Joint Propulsion Conference & Exhibit, Tucson, AZ, July 10 – 13, 2002

Enomoto N., Kim J.-H., Ishizaka K., Watanabe S. & Furukawa A., "Suppression of Cavitation Surge of a Helical Inducer Ocurring in Partial Flow Conditions," OS-4-003, 5th International Symposium on Cavitation (CAV 2003), Osaka, Japan, November 1-4, 2003

Fujii, A., Azuma, S., Yoshida, Y., Tsujimoto, Y., Horiguchi, H., and Watanabe, S., 2002, "Higher Order Rotating Cavitation in an Inducer," The 9th of International Symposium on Transport Phenomena and Dynamics of Rotating Machinery, Honolulu, Hawaii.

Furukawa, A., Ishizaka, K., and Watanabe, S., 2001, "Experimental Estimate of Helical Inducer Blade Force in Cavitation Surge Condition.", Proceeding of 4th International Symposium on Cavitation, Pasadena, California

Horiguchi, H., Watanabe, S., & Tsujimoto, Y., "Theoretical Analysis of Cavitation in Inducers with Unequal Blades with Alternate Leading Edge Cutback: Part I- Analytical Methods and the Results for Smaller Amounts of Cutback." Journal of Fluids Eng., Vol. 5, 2000

Imamura H., Kurokawa J., Matsui J., & Kikuchi M., "Suppression of Cavitating Flow in Inducer by J-Groove," OS-4-006, 5th International Symposium on Cavitation (CAV 2003), Osaka, Japan, November 1-4, 2003.

Kim, J-H., et al., "Suppression of Cavitation Surge of Pump Inducer by Inserting Ring-Shaped Inlet Plate", 6th International Symposium on Cavitation (CAV2006), Wageningen, The Netherlands, September 2006

Ono A., Warashina S., Tomaru H., Oguchi H., "Development of Cryogenic Turbopumps for the LE-7A Engine,", Vol. 37 No. 1 February.

Rebattet C., Wegner M., Morel P., & Bonhomme C., "Inducer Design that Avoids Rotating Cavitation," AFI 2001-WS10, Oct. 5, 2001.

Shimiya, N. et al., "Suppression of Cavitation Instabilities in an Inducer by J-Groove", 6th International Symposium on Cavitation (CAV2006), Wageningen, The Netherlands, September 2006

Shimura T., Shimagaki M., Watanabe Y., Watanabe M., Hasegawa S., & Takata S., "Cavitation Induced Vibration of LE-7A Oxygen Turbopump," OS-4-009, 5th International Symposium on Cavitation (CAV 2003), Osaka, Japan, November 1-4, 2003.

Stripling, L.B and Acosta, A.J., Cavitation in Turbopumps – Part 1, ASME Transaction, Sept. 1962, 326-338

Stripling, L.B and Acosta, A.J., Cavitation in Turbopumps – Part 2, ASME Transaction, Sept. 1962, 339-50

Subbaraman, M., & Burton, K., "Cavitation-Induced Vibrations in Turbomachinery: Water Model Exploration," OS-4-013, 5th International Symposium on Cavitation (CAV 2003), Osaka, Japan, November 1-4, 2003

Subbaraman, M. and Patton, M., "Suppressing Higher Order Cavitation Phenoemena in Axial Inducers", 6th International Symposium on Cavitation (CAV2006), Wageningen, The Netherlands, September 2006

Tsujimoto, Y., 2001, "Simple Rules for Cavitation Instabilities in Turbomachinery."Invited Lecture 06, Proceeding of 4th International Symposium on Cavitation, Pasadena, CA

Tsujimoto, Y., Yoshida, Y., Maekawa, Y., Watanabe, S., and Hashimoto, T., 1997, "Observations of Oscillating Cavitations of an Inducer," ASME Journal of Fluids Engineering, Vol. 119, No. 4, 775-781.

Yoshida Y., Tsujimoto Y., Kataoka D., Horiguchi H., & Walh, F., "Effects of Alternate Leading Edge Cutback on Unsteady Cavitation on 4-Bladed Inducers," Journal of Fluids Engineering Transactions of the ASME). Vol 123, no.4, pp. 762-770. Dec. 2001.